A Single Waveguide Spectrometer via Defect Scattering

Xue Tong, Zhenning Zhao, Yunxian Zhong, Dong Lin, Zhuangzhuang Zhu, Qing Zhong, and Jinping He

***Abstract*—Miniaturized spectrometers show great application potential in biology, medicine, astronomy and so on. However, it is still challenging to obtain broadband spectrum and high spectral resolution simultaneously with limited size. In this study, we proposed a single waveguide spectrometer based on light scattering of the defects buried in the waveguide. The detections of the scattering light are set on the upper surface of the waveguide, as a result, tremendous detection channels can be realized even within a small structure size, which makes simultaneously high resolution and broad bandwidth detection achievable. Simulation studies show that this kind of spectrometer can exhibits an impressive bandwidth of 1000 nm, ranging from 600 to 1600 nm. Additionally, a resolution of 0.2 nm is achieved within the range of 850 to 852 nm through fine sampling. The influence factors of the performance of the spectrometer is also studied. This work provides the possibility of achieving on-chip, high-resolution, and wide-bandwidth spectrometers.**

***Index Terms*—Miniaturized spectrometer, waveguide, reconstruction spectrometer.**

I. Introduction

SPECTROMETER plays a crucial role in numerous applications, such as astronomical detection [1], biological and chemical characterization [2], as well as material analysis [3], among others. Presently, there is increasing attention towards miniaturized spectrometers due to their compact size, light weight, and low energy consumption [4]. As a result, two major categories of miniaturized spectrometers have emerged. The first category is based on on-chip dispersion, such as Arrayed Waveguide Gratings (AWG) [5], [6], [7] and on-chip echelle gratings spectrometers [8]. The second category is based on on-chip Fourier transform, exemplified by Stationary Wave Integrated Fourier Transform Spectrometers (SWIFTS) [9], [10]. Both types of spectrometers possess relatively small dimensions. However, the principles underlying these spectrometers are similar to traditional spectrometers. To achieve higher resolution, the footprints must be larger. This has not overcome the constraint between size and resolution, imposing limitations on the design of ultra-compact spectrometers [11].

In recent years, a novel type of spectrometer, known as the reconstruction spectrometers, has emerged, incorporating algorithms to overcome traditional constraints in terms of resolution and size. Its operational principle involves utilizing devices or structures with spectral responses to establish a mapping relationship between the spectrum and the signals detected. This relationship is stored in a transfer matrix. Through pre-calibration to obtain the transfer matrix, the input spectrum can be reconstructed from the detected signals. Structures with wavelength-dependent characteristics, such as quantum dots [12], disordered scattering media [13], photonic crystal-based filter arrays [14], and even single-nanowires [15], have been proposed and validated for reconstruction spectrometers. Typically, in this kind of spectrometer, the incident light is dispersed into different detection channels, and the quantity of the effective detection channels significantly influences the performance of the spectrometer. A small number of detection channel means inadequate sampling and result in poor performance, such as low resolution, low accuracy and narrow bandwidth. The detection channels of the structures mentioned above are typically several to several tens, which is far from efficient sampling to obtain high quality spectrum.

To obtain sufficient detection channels with minimized structure size, we propose a single waveguide spectrometer based on light scattering of defects. The defects are arranged on the surface of the waveguide, disrupting the stable transmission of light through the waveguide and scattering the light out from the upper surface. This design can obtain thousands of detection.

II. Principle

The principle of the spectrometer is proposed by us firstly. The spectrometer is based on MMI interference and defect scattering, which can introduce a wavelength-dependent intensity distribution, and help to obtain a better performance compared with other spectrometers of only one wavelength-dependent process.

Received 20 February 2025; revised 18 March 2025; accepted 19 March 2025. Date of publication 24 March 2025; date of current version 10 April 2025. This work was supported in part by the National Natural Science Foundation of China under Grant 11973009 and Grant 11933005, in part by the Jiangsu Provincial Key Research and Development Program under Grant BE2023080, and in part by the Chinese Academy of Sciences under Grant KGFZD-145-23-04-03. *(Xue Tong and Zhenning Zhao are co-first authors.) (Corresponding author: Jinping He.)*

Xue Tong, Zhenning Zhao, Yunxian Zhong, Dong Lin, Zhuangzhuang Zhu, and Qing Zhong are with the Laboratory of Solar and Space Instruments, Nanjing Institute of Astronomical Optics & Technology, Chinese Academy of Sciences, Nanjing 210042, China, also with the CAS Key Laboratory of Astronomical Optics & Technology, Nanjing Institute of Astronomical Optics & Technology, Chinese Academy of Sciences, Nanjing 210042, China, also with the University of Chinese Academy of Sciences, Nanjing 211135, China, and also with the University of Chinese Academy of Sciences, Beijing 100049, China.

Jinping He is with the Laboratory of Solar and Space Instruments, Nanjing Institute of Astronomical Optics & Technology, Chinese Academy of Sciences, Nanjing 210042, China, also with the CAS Key Laboratory of Astronomical Optics & Technology, Nanjing Institute of Astronomical Optics & Technology, Chinese Academy of Sciences, Nanjing 210042, China, and also with the University of Chinese Academy of Sciences, Nanjing 211135, China (e-mail: jphe@niaot.ac.cn).

Digital Object Identifier 10.1109/JPHOT.2025.3554022

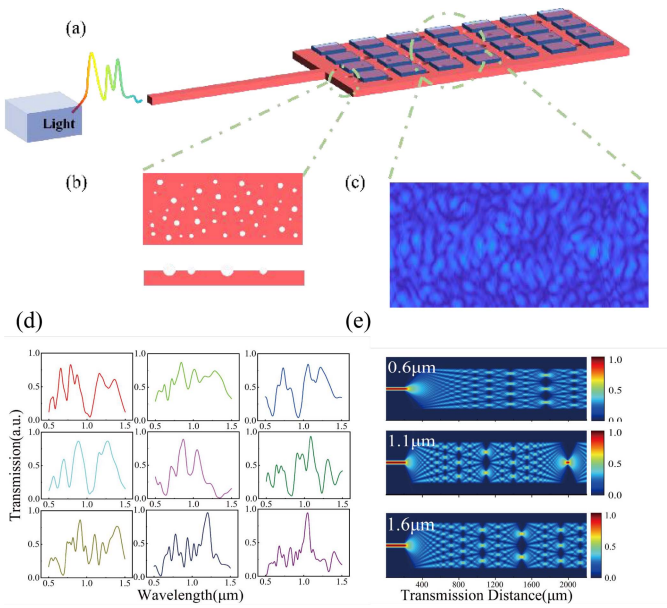

Fig. 1. Principle of the spectrometer. (a) Schematic of our proposed single waveguide spectrometer, (b) an example of the distribution of surface defects on waveguides, (c) light field distribution detected on the upper surface of the waveguide, (d) response spectra for some of the defects. The response intensities vary depending on the positions of defects within the waveguide, (e) multimode interference at wavelengths of 0.6 μm, 1.1 μm, and 1.6 μm.

Fig. 1 shows the principle of the proposed spectrometer. Fig. 1(a) demonstrates the schematic of the single waveguide spectrometer. A single-mode waveguide is used to couple the light into the spectrometer and obtain a stable field distribution. Then, the light progresses into the multimode waveguide, which serves as the wavelength-dependent signal generation and detection region. As shown in Fig. 1(b), the wavelength-related light scattering occurs due to the random distributed defects on the surface of the multimode waveguide.

Subsequently, the wavelength-related scattered optical signals can be captured with a two-dimension detector set on the upper surface of the multimode waveguide [shown in Fig. 1(c)]. The detection efficiency is about 26.3% . A more detailed energy distribution and efficiency calculation can be found in Supplementary Material S1. Since two wavelength-related physical processes (multimode interference and light scattering) exist in the signal generation process, the signal (light distribution on the upper surface) has a very high wavelength sensitivity, which will help to obtain high performance spectra. The spectral responses at 9 different positions on the multimode waveguide are shown in Fig. 1(d), and we can find that there are sharp peaks and fine structures in all curves. In addition, the multimode-interference will induce the wavelength-dependent field distribution are shown in Fig. 1(e), which prove the high wavelength sensitivity. What should be mentioned is that the signal detection is set on the upper surface of the multimode waveguide, as a result, thousands of detection channels can be obtained with a single multimode waveguide with width of several μm and length of 5 mm.

The spectrometer based on this design consists primarily of two processes: light intensity detection and algorithm reconstruction. The light intensity detection process helps to obtain the wavelength-related information, and the spectrum can be reconstructed with the process of algorithm reconstruction. The scattered light distributions are captured by a 2D detector. Following the calibration of the spectrometer, the original spectral information of the incident light can be obtained through a reconstruction algorithm.

The intensity of the scattered light distributions [as shown in Fig. 1(c)] can be represented by the following mathematical formula:

$$\mathrm{I(x,y)} = \int \mathrm{p\,(x,y,\lambda)\,R\,(x,y,\lambda)\ S\,(\lambda)\,d\lambda} \tag{1}$$

where I(x,y) is the intensity distributions of the scattered light on the detector; p(x,y,λ) represents the response of the optical system, and R(x,y,λ) is the response of the detector. S(λ) stands for the spectrum of the incident light. We set the response of the whole system as $T\ (x,y,\lambda) =\ p(x,y,\lambda)R(x,y,\lambda)$, then the intensity distributions of the scattered light can be written as

$$I\ (x,y) = \int T\,(x,,y,\lambda)\ S\,(\lambda)\,d\lambda \tag{2}$$

T(x,y,λ) is the total scattering transmission function. In matrix algebra formalism, a discretized transmission matrix, T(x,y,λ) can be obtained by discretization of the spectral and spatial components, yielding:

$$\begin{pmatrix} T_{11} & \cdots & T_{m1} \\ \vdots & \ddots & \vdots \\ T_{1n} & \cdots & T_{mn} \end{pmatrix} \begin{bmatrix} S_1 \\ \vdots \\ S_m \end{bmatrix} = \begin{bmatrix} I_1 \\ \vdots \\ I_n \end{bmatrix} \tag{3}$$

m and n represent the number of channels for spectral and spatial light spots, respectively. T_n is the transmittance function of the *n* spatial light spot channel, T_m is the transmission matrix of the *m* spectral channel, S_m represents the intensity of the *m* spectral component of the incident light, and I_n is the light field intensity at the *n* pixel on the photodetector corresponding to the *n* spatial light spot channel.

The spectrometer requires calibration before taking measurements, and the transmission matrix T(x,y,λ) needs to be determined to establish the mapping relationship between the light spot and the wavelength. By inputting monochromatic light S_m with a known wavelength, the detector can capture the corresponding light intensity distribution, I(x,y). Continuously changing the wavelength of the input light source enables the acquisition of a collection of light spot patterns corresponding to various wavelengths. Subsequently, T(x,y,λ) is determined sequentially.

After calibrating the transmission matrix T(x,y,λ), spectral information of the incident light can be obtained by solving a system of linear equations in reverse, as demonstrated in the following formula [16]:

$$\mathrm{S}\ = T^{-1}\ I \tag{4}$$

In order to prevent (3) from becoming ill-conditioned, the spectral channels in the transmission matrix, i.e., the spacing between adjacent wavelengths, should not be smaller than the spectral resolution determined by the system. After calibration,

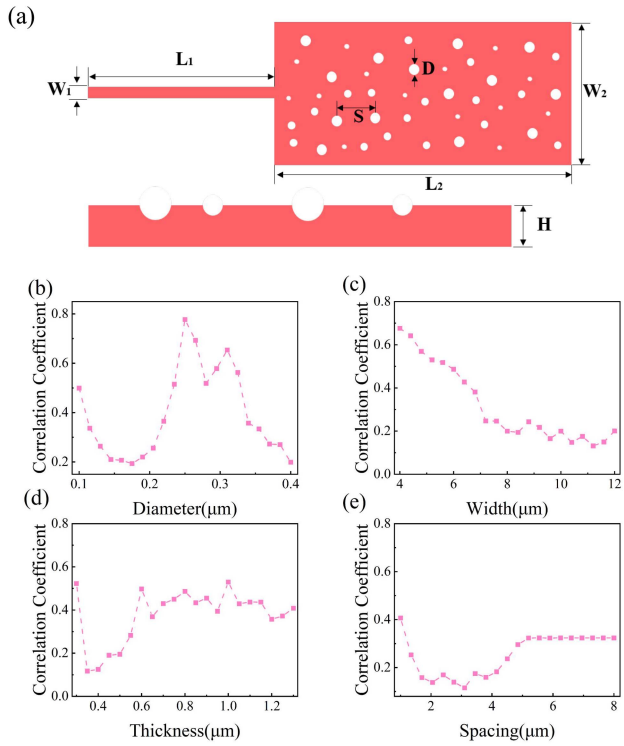

Fig. 2. Spectrometer design and optimization. (a) Schematic diagram of single-waveguide spectrometer plane. (b) Variations in the correlation coefficient with different defect diameters, and the favorable range is 0.1-0.23 μm. (c) The impact of waveguide width and the suitable range is greater than 7 μm. (d) The influence of waveguide thickness and the favorable range is 0.35-0.55 μm. (e) The impact of defect spacing, the entire range satisfies the correlation requirements, with the optimal range being 1–5 μm.

measures should be taken to minimize alterations in the transmission matrix caused by environmental factors. Utilizing the equation $\mathrm{S} = T^{-1} I$, in conjunction with Tikhonov regularization, allows for the recovery of an approximate spectral signal S(λ) corresponding to the incident spectrum.

III. Design

A single waveguide spectrometer based on the defects scattering is designed and subsequently optimized. As illustrated in Fig. 2(a), the two-dimensional scattering structure consists of a random array of hemispherical silica holes etched into a silicon nitride waveguide. The resolution of the spectrometer depends on the minimum wavelength change required to produce a weakly correlated intensity distribution. This is expressed using a correlation function. It can be estimated using a correlation function:

$$\mathrm{C}(\Delta\lambda) = \frac{\langle I(\lambda, x) I(\lambda + \Delta\lambda, x)\rangle}{\langle I(\lambda, x) I(\lambda + \Delta\lambda, x)\rangle} - 1 \tag{5}$$

where I(λ,x) represents the light intensity distribution generated by detector x at wavelength λ, and $\langle\cdots\rangle$ denotes the average value at wavelength λ. As the correlation between the light fields produced by two wavelengths decreases, it becomes easier for the algorithm to distinguish between them, leading to improved reconstruction accuracy. The correlation function $\mathrm{C}(\Delta\lambda)$ can be optimized through four variables, diameters (D), waveguide width (W2), waveguide thickness (H), and defect spacing (S). During optimization, we ensure that the correlation between light fields from each pair of wavelengths across the entire range approaches a value below 0.5 as closely as possible. The average correlation can be calculated from the correlation matrix, and subsequent parameter optimization can be performed based on this calculated average correlation.

The algorithm we use is Finite Difference Time Domain (FDTD), where a random array is generated using a random algorithm and does not follow any distribution. The specific simulation parameters are as follows: the waveguide configuration is shown in Supplementary Material S2, with a silicon substrate (refractive index of 3.45), a silicon nitride core layer (refractive index of 1.99), and a silicon dioxide cladding layer (refractive index of 1.45). The size of the TM_0 mode of the waveguide is 3 μm for the wavelength of 1600 nm, in which case the mode field is at its maximum for the spectral range of 600 nm∼1600 nm. The gap between the silicon nitride core and the silicon substrate is set as 10 μm, which is much larger than the mode size, resulting in the mode leakage into the silicon substrate less than 1% . In this case, the significant optical absorption of the silicon substrate for the wavelength below 1100 nm will not influence the effciency and bandwidth of the spectrometer largely.

After a series of computations, the approximate range of parameters is obtained and further optimized is performed within this range. Indeed, we have simulated many other defect shapes, such as triangle, rectangle and so on, and the shape does not influence the performance largely since the size of the defects is relatively small. So, we use a shape hemisphere as a representative. When optimizing the diameter, the optimal initial structure selected is a waveguide thickness of 0.5 μm, width of 8 μm, and spacing of 1.5 μm. As illustrated in Fig. 2(b), the appropriate diameter range for the defects is between 0.1 μm and 0.23 μm. Although the correlation decreases sharply to less than 0.2 when the particle size exceeds 0.4 μm, this decrease is attributed to strong scattering, which leads to rapid dissipation of light energy. The specific relationship between particle diameter and energy dissipation can be examined in Supplementary Material S3. Consequently, signal detection is limited to a narrow range, resulting in fewer detection channels and ultimately leading to poor performance in spectrum detection. When optimizing the width and thickness, the diameter is selected as 0.2 μm and the column spacing is 1.5 μm. As shown in Fig. 2(c) and (d), the recommended waveguide thickness ranges from 0.35 μm to 0.55 μm, while a waveguide width exceeding 7 μm is found to be optimal. In the case of the overall defect array on the waveguide, the selected thickness is 0.5 μm, width is 8 μm, and diameter is 0.2 μm, as depicted in Fig. 2(e), the spacing of the defects has a relatively minor impact on the performance, with the optimal range being 1 to 5 μm.

Based on the above simulation results, we have determined the optimal parameters of the spectrometer based on defect scattering. The position of the defect is the offset relative to the center of the waveguide. It is worth mentioning that in order to obtain better results, we have also added random variables to some parameters, and the random quantities are selected within

TABLE I
PARAMETERS OF THE SINGLE WAVEGUIDE SPECTROMETER

Parameters	Standard value	Random quantity
Length	4500 μm	\
Width	8 μm	\
Thickness	0.5 μm	\
Diameter	0.15 μm	0.05 μm
Spacing (X direction)	1.7 μm	1 μm
Spacing (Y direction)	3 μm	1.5 μm

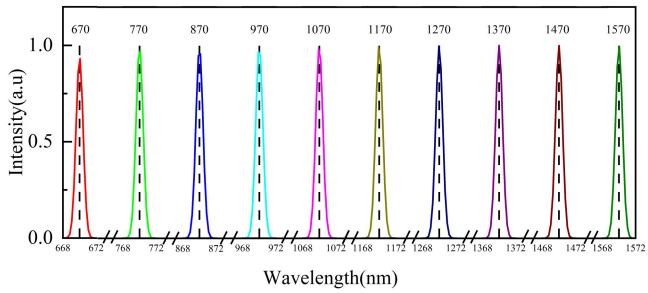

Fig. 3. Results of broadband spectral reconstruction. Reconstructed spectra for a series of narrowband spectral lines, and single peaks across the entire spectrum range can be reconstructed. The black dashed lines mark their center wavelengths.

the optimized parameter range. The specific parameters of the spectrometer are shown in Table I:

IV. RESULTS AND DISCUSSIONS

A. The Performance of the Single-Waveguide Spectrometer

To test the performance of the single-waveguide spectrometer, ten equal intensity unimodal signals with wavelengths ranging from 600 nm to 1600 nm was set up. The first peak exhibited a center wavelength of 670 nm, whereas the subsequent peaks were spaced at regular intervals of 100 nm. Gaussian noise was added to the distribution, and spectral reconstruction was conducted with a signal-to-noise ratio of 20 dB. As shown in Fig. 3, the single-peak signal within the entire 1000 nm range can be accurately reconstructed. It can be observed that there is commendable performance at long wavelengths, primarily manifested by intensity reconstruction. When dealing with scattering structures, shorter wavelengths cause quick dissipation of energy, leading to a smaller observable region and faster depreciation of optical field energy. In contrast, longer wavelengths undergo a slower decrease, resulting in better reconstruction outcomes. It is worth noting that 600–1600 nm is the optimal value for this waveguide configuration and material, and similar performance may also be observed in shorter or longer wavelengths, which requires other optimization parameters such as material and waveguide size.

To measure the resolution of the single-waveguide spectrometer, the wavelength range of 600–1600 nm was divided into five segments with 200 nm intervals: 600–800 nm, 800–1000 nm,

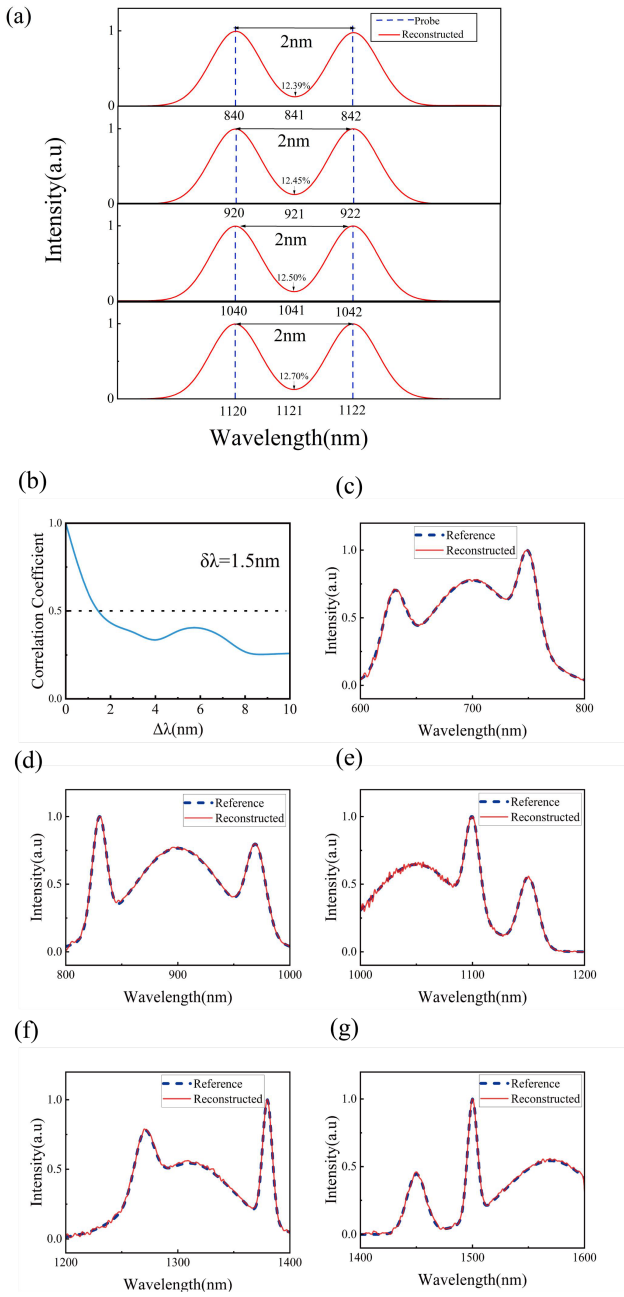

Fig. 4. Results of broadband spectral reconstruction. (a) Reconstruction results of dual-peak spectra in the 800–1000 nm and 1000–1200 nm bands. Within both wavelength bands, it can effectively distinguish dual peaks with a separation of 2 nm. (b) Correlation coefficients for spectra across all bands (600–1600 nm). The half-width at half-maximum is 1.5 nm, meaning a wavelength shift of 1.5 nm reduces the degree of spectral correlation to half. (c) –(g) Reconstructed spectrum for a continuous, broadband spectra. This single-waveguide spectrometer exhibits commendable reconstruction accuracy.

1000–1200 nm, 1200–1400 nm, and 1400–1600 nm, constrained by simulation conditions such as computational duration, and the transmission matrix is also obtained from five bands separately. As shown in Fig. 4(b), it is demonstrated that for the single-waveguide spectrometer, the half-width at half-maximum, $\delta\lambda$, was found to be 1.5 nm. This signifies that a wavelength shift of 1.5 nm is sufficient to reduce the correlation of the optical field patterns to 0.5. $\delta\lambda$ serves as an estimate of the spectral resolution,

given the impossibility of resolving two wavelengths with highly correlated optical field patterns. More detailed cross-correlation between channels is provided in Supplementary Material S4, and the value is typically less than 0.5.

The optical field correlation function can only provide an estimate of spectral resolution, while the actual resolution of a single-waveguide spectrometer is determined by the smallest wavelength interval it can distinguish. In five spectral bands, dual peaks with a spacing of 2 nm are arranged, each pair separated by 40 nm, with equal intensities. Subsequently, we conducted tests on the minimum resolvable wavelength spacing for five distinct spectral bands, revealing a consistent minimum resolvable wavelength spacing of 2 nm within each respective band. Here, we present the results for the 800–1000 nm and 1000–1200 nm spectral bands and the resolution is better than 2 nm, shown in Fig. 4(a).

In addition, it is necessary to reconstruct a broadband, continuous spectrum to verify the performance of the single-waveguide spectrometer. Similar to the methodology employed for resolution assessment, we reconstructed various broadband spectra within the five spectral bands, and the spectra of different shapes are generated by algorithms, yielding satisfactory reconstruction results, as illustrated in Fig. 4(c)–(g). It can be concluded that spectra can be reconstructed well in all five bands. It is worth noting that across all spectral bands, we observed that the reconstruction results for narrow peaks outperform those for flat spectra, with this effect being particularly pronounced in the 1000–1200 nm wavelength range. Within the 1000–1200 nm segment, an increase in noise is observed particularly in the 1000–1100 nm sub-segment. As a general trend, reconstruction has been demonstrated to be more effective for narrow peaks, while broader peaks induce higher levels of reconstruction noise.

In conducting optical field correlation analysis on the broad wavelength range, we observed enhanced performance of the single-waveguide spectrometer within certain narrow bands. Due to simulation constraints, a detailed analysis across the entire wavelength range was not performed. Instead, detailed simulations were conducted specifically on the 800–1000 nm spectral band, where the single-waveguide spectrometer demonstrated superior performance. Within the range of 800–1000 nm, calculations were carried out with a smaller step size of approximately 0.1 nm, and the results, as shown in Fig. 5(a), indicate optimal performance at 850–852 nm, where the correlation coefficient decreases to 0.5 at a wavelength difference ($\delta\lambda$) of 0.13 nm. Following that, tests were carried out to assess the ability of the system to distinguish dual peaks, resulting in the determination of a minimum resolvable gap of 0.2 nm between the dual peaks. Hence, the ultimate resolution of this single-waveguide spectrometer is established at 0.2 nm.

B. Discussions on Factors Affecting Detection

1) The Impact of the Detection Region: In the overall design of the spectrometer, the detector array is placed directly adjacent to the waveguide surface. Fig. 6 shows that the light with short wavelength is scattered out faster than that of the longer wavelength. This phenomenon will help to enhance the

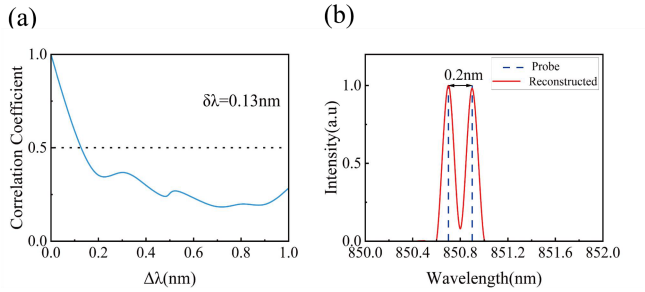

Fig. 5. Results of limiting resolution. (a) Correlation coefficients for spectra in a narrow band (850–852 nm). The half-width at half-maximum is 0.13 nm, meaning a wavelength shift of 0.13 nm reduces the degree of spectral correlation to half. (b) Reconstruction results of dual-peak spectra in the 850–852 nm. It can effectively distinguish dual peaks with a separation of 0.15 nm.

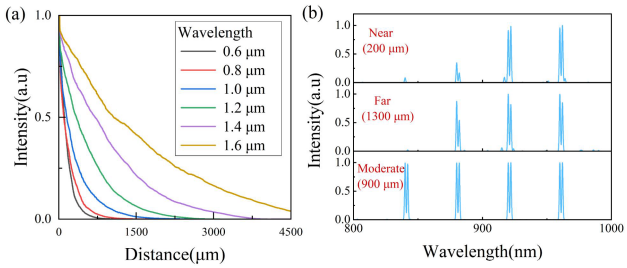

Fig. 6. The impact of the detection region on spectral reconstruction. (a) The correlation between the detected spectral intensity and the distance of light transmission at various wavelengths. (b) Results of spectral reconstruction under various detection regions.

performance of the spectrometer. However, it also increases the complexity of the reconstruction process, since we need to choose the appropriate reconstruction region for different spectral range. Within the entire optical field of the multimode waveguide, the region nearer to the light source experiences minimal disruption from defects but is notably influenced by the light source itself. While this region exhibits higher energy, its correlation is excessively high, which is unfavorable for spectral reconstruction. On the contrary, at the end of the waveguide, there is energy dissipation, and the signal is more susceptible to noise, making it less conducive to effective detector collection. Therefore, the selection of an appropriate detection region is crucial.

As shown in Fig. 6(a), shorter wavelengths lead to quicker energy dissipation. At 600 nm, the transmission distance is only about 500 μm before the energy becomes nearly imperceptible. This highlights that the spectrometer may not be suitable for wavelengths below 600 nm, potentially reaching the short-wavelength limit of the silicon nitride waveguide. In such scenarios, the detectable area is more confined, resulting in fewer data points and impacting the accuracy of spectral reconstruction. Furthermore, the region with lower energy levels near the end of the waveguide is also less conducive to effective detection [shown in Fig. 6(b)]. Therefore, in the exploration of different wavelength ranges, it is essential to conduct preliminary energy detection, followed by the selection of appropriate regions for further analysis. During the calibration process, a critical aspect is to comprehend the spectral response generated by the entire

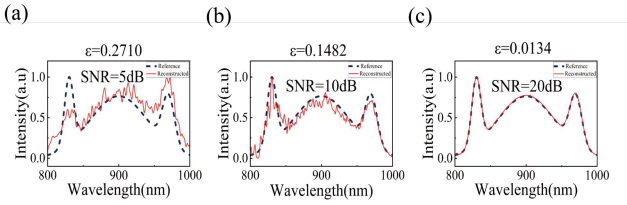

Fig. 7. Results of spectral reconstruction at various signal-to-noise ratios. (a) Reconstruction results at 5 dB. (b) Reconstruction results at 10 dB. (c) Reconstruction results at 20 dB.

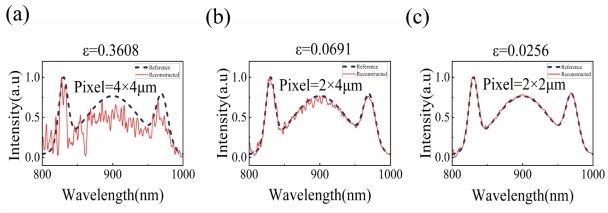

Fig. 8. Results of spectral reconstruction under varying sampling conditions. (a) Reconstruction results at 4 × 4 μm. (b) Reconstruction results at 2 × 4 μm. (c) Reconstruction results at 2 × 2 μm.

single-waveguide spectrometer and choose suitable detection regions within different wavelength ranges, preferably areas with strong energy and low correlation.

2) Impact of Signal-to-Noise Ratio on Reconstruction: In spectral reconstruction, the influence of signal-to-noise ratio (SNR) is crucial, which determines whether the single-waveguide spectrometer has the potential for practical applications in detection. To assess the accuracy of the reconstruction, the relative reconstruction error can be calculated as follows [17]:

$$\varepsilon = \frac{\left[\sum_{i=1}^{N}(S - S_0)^2\right]^{1/2}}{\left(\sum_{i=1}^{N}(S_0{}^2)\right)^{1/2}} \tag{6}$$

where S denotes the reconstructed spectrum, S_0 is the original spectrum, and N represents the total number of spectral samples. As shown in Fig. 7(a)–(c), when the signal-to-noise ratio is 5 dB, partial spectral features can be reconstructed, especially under conditions of long wavelengths. As the signal-to-noise ratio increases to 10 dB, the spectral noise becomes relatively pronounced. Although the spectral shape can generally be recovered, there is an excessive amount of noise in the signal. As the spectral shape becomes more complex, it tends to obscure the true signal. However, when the signal-to-noise ratio further increases to 20 dB, the spectral reconstruction results improve significantly. Therefore, when the requirement for reconstruction accuracy is not stringent, such as in the case of seeking characteristic peaks, a signal-to-noise ratio of 10 dB is generally sufficient to meet preliminary requirements. When the signal-to-noise ratio reaches 20 dB, the spectral reconstruction results tend towards perfection, making it suitable for scenarios demanding higher precision.

3) Impact of Sampling on Reconstruction: This type of random scattered spectrometer has the capability to transform each output signal into N distinct, uncorrelated yet deterministically defined signals on different channels. Mathematically, this process is analogous to decomposing the input signal into N orthogonal spectra. Therefore, the accuracy of spectral reconstruction is closely related to N. As shown in Fig. 8(a)–(c), under the condition of 4 × 4 μm sampling, the spectral noise becomes quite pronounced, posing a challenge in distinguishing between signal and noise. However, despite this, it is still possible to reconstruct partial spectral features, especially the peak values. With 2 × 4 μm sampling, the spectral shape can be essentially reconstructed, although there is slight noise interference. 2 × 2 μm sampling yields a better reconstruction of the spectral shape, characterized by minimal noise. Therefore, when the requirement for reconstruction accuracy is not stringent, such as when seeking characteristic peaks, a 2 × 4 μm sampling rate is generally sufficient to meet preliminary requirements. When the sampling rate is increased to 4 × 4 μm, the spectral reconstruction results tend towards perfection, making it suitable for high-precision applications.

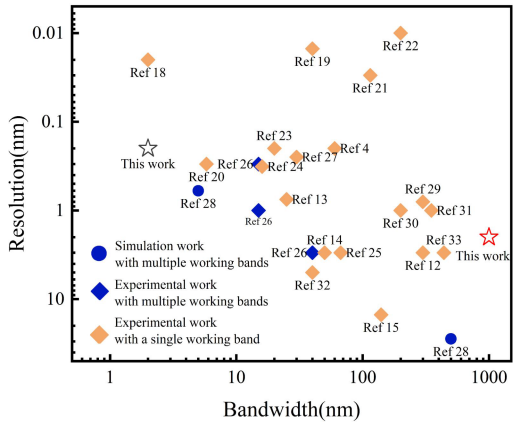

Fig. 9. Performance comparison with construction spectrometers. This spectrometer demonstrates a significant advantage in terms of bandwidth, particularly within the 1000 nm range.

C. Performance Comparison With Other Construction Spectrometers

To emphasize the advantages of this study, we conducted comparisons with recent notable works [4], [12], [13], [14], [15], [18], [19], [20], [21], [22], [23], [24], [25], [26], [27], [28], [29], [30], [31], [32], [33]. Fig. 9 illustrates the performance of computational reconstruction spectrometers in terms of resolution and bandwidth, which are critical metrics for assessing the quality of a spectrometer. Specifically, we selected works that underwent resolution testing, i.e., those capable of resolving the narrowest dual peaks, and demonstrated performance across the entire bandwidth. It is evident that our work holds a significant advantage in terms of bandwidth, achieving an impressive 1000 nm, with further potential for enhancement. Furthermore, following calibration, this approach requires only a single measurement for spectral reconstruction, in contrast to many existing methods that rely on narrow-band filtering,

necessitating longer sampling times and precise voltage or temperature control. Therefore, we can anticipate that this study holds considerable potential.

D. Discussion on Experimental Implementation

The silicon nitride single mode and multi-mode waveguides can be fabricated with LPCVD (Low Pressure Chemical Vapor Deposition) and photolithography. Since the performance of the spectrometer has relatively large tolerance of the size and shape of the defects, the hemispherical defects can be produced through laser micro-nano machining [34]. And, defects of different sizes can be fabricated by thermal reflow [35], and the combination of thermal reflow and other processes can reduce the diameter of silicon nitride to as small as 30 nm [36]. In addition, photodetectors, such as CVD graphene and Si, can be integrated on the waveguides [37], [38], which makes the spectrometer smaller and more stable. But the on chip integrated two-dimensional spatial light photodetectors still poses challenges currently. A more feasible experimental approach to achieve efficiently two-dimensional detection of the scattering light could be mechanically fixing of two-dimensional CCD/CMOS detector chip on the surface of the optical chip, or the integration of the detectors with the optical chip using CMOS compatible technologies [39], [40], [41].

The spectrometer consists of MMI and defects. MMI structures without defects is a very mature photonic device that is very easy to process. Defects are also easily obtainable, so our structure is easy to process.

V. Conclusion

In this study, we have proposed a new detection method based on a single waveguide and designed the structure and conducted simulation optimization. As a result, the single-waveguide spectrometer is based on multimode-interference with the defect scattering. And it is characterized by its compact structure and cost-effectiveness. Moreover, there is more ample sampling due to detection on the upper surface of the waveguide, leading to enhanced performance. We achieved 2 nm resolution in the wavelength range of 600–1600 nm. Furthermore, it is noteworthy that the single-waveguide spectrometer exhibits superior performance in specific narrow bands due to finer sampling, i.e., in the wavelength range of 850 nm to 852 nm, it can reach a resolution of 0.2 nm. During the optimization process, we discovered that the spectrometer has a relatively high tolerance for manufacturing errors, given its basis on random scattering. Therefore, there should be no significant challenges in the fabrication process. Additionally, we discussed various influencing factors and found that the requirements for practical detection with our spectrometer are not excessively stringent. Consequently, this single waveguide spectrometer has great potential in on-site spectral analytical applications such as on-chip chemical and biological sensing.

References

[1] S.-H. Lee et al., "Multidetector grating spectrometer for infrared astronomy," *Proc. Nat. Acad. Sci. USA*, vol. 109, pp. 17436–17441, 1986.

[2] M. J. Rust, M. Bates, and X. Zhuang, "Ultrasensitive nanophotonic random spectrometer with microfluidic channels as a sensor for biological applications," *Nat. Methods*, vol. 3, pp. 793–796, 2022.

[3] K. K. Bearne et al., "A modified traveling wave ion mobility mass spectrometer as a versatile platform for gas-phase ion-molecule reactions," *Opt. Exp.*, vol. 29, pp. 11784–11792, 2019.

[4] C. Sun et al., "Integrated microring spectrometer with In-hardware compressed sensing to break the resolution-bandwidth limit for general continuous spectrum analysis," *Laser Photon. Rev.*, vol. 17, 2023, Art. no. 2300291.

[5] M. K. Smit, "New focusing and dispersive planar component based on an optical phased array," *Electron. Lett.*, vol. 24, pp. 385–386, 1988.

[6] P. Gatkine et al., "Arrayed waveguide grating spectrometers for astronomical applications: New results," *Opt. Exp.*, vol. 25, pp. 17918–17935, 2017.

[7] D. Lin et al., "Research progress of high-resolution arrayed waveguide spectroscopy," in *Proc. Novel Technol. Instrum. Astron. Multi-Band Observ.*, 2021, pp. 284–289.

[8] D. Melati et al., "Compact and low crosstalk echelle grating demultiplexer on silicon-on-insulator technology," *Electronics*, vol. 8, 2019, Art. no. 687.

[9] E. le Coarer et al., "Wavelength-scale stationary-wave integrated fourier-transform spectrometry," *Nature Photon.*, vol. 1, pp. 473–478, 2017.

[10] J. Bland-Hawthorn and P. Kern, "Molding the flow of light: Photonics in astronomy," *Phys. Today*, vol. 65, pp. 31–37, 2012.

[11] R. F. Wolffenbuttel, "State-of-the-art in integrated optical microspectrometers," *IEEE Trans. Instrum. Meas.*, vol. 53, no. 1, pp. 197–202, Feb. 2004.

[12] J. Bao and M. Bawendi, "A colloidal quantum dot spectrometer," *Nature*, vol. 523, pp. 67–70, 2015.

[13] B. Redding et al., "Compact spectrometer based on a disordered photonic chip," *Nature Photon.*, vol. 7, pp. 746–751, 2013.

[14] N. Sharma et al., "Reconstructive spectrometer using a photonic crystal cavity," *Opt. Exp.*, vol. 29, pp. 26645–26657, 2021.

[15] Z. Y. Yang et al., "Single-nanowire spectrometers," *Science*, vol. 365, pp. 1017–1020, 2019.

[16] B. Redding, S. M. Popoff, and H. Cao, "All-fiber spectrometer based on speckle pattern reconstruction," *Opt. Exp.*, vol. 21, pp. 6584–6600, 2013.

[17] Z. Zhang et al., "Compact high resolution speckle spectrometer by using linear coherent integrated network on silicon nitride platform at 776 nm," *Laser Photon. Rev.*, vol. 15, 2021, Art. no. 2100039.

[18] M. Piels and D. Zibar, "Compact silicon multimode waveguide spectrometer with enhanced bandwidth," *Sci. Rep.*, vol. 7, 2017, Art. no. 43454.

[19] Z. J. Lin et al., "High-performance, intelligent, on-chip speckle spectrometer using 2D silicon photonic disordered microring lattice," *Optica*, vol. 10, pp. 497–504, 2023.

[20] D. Yi, Y. Zhang, X. Wu, and H. K. Tsang, "Integrated multimode waveguide with photonic lantern for speckle spectroscopy," *IEEE J. Quantum Electron.*, vol. 57, no. 1, Feb. 2021, Art. no. 0600108.

[21] C. Yao et al., "Broadband picometer-scale resolution on-chip spectrometer with reconfigurable photonics," *Light. Sci. Appl.*, vol. 12, 2023, Art. no. 156.

[22] C. Yao et al., "Integrated reconstructive spectrometer with programmable photonic circuits," *Nat. Commun.*, vol. 14, 2023, Art. no. 6376.

[23] C. Sun et al., "Scalable on-chip microdisk resonator spectrometer," *Laser Photon. Rev.*, vol. 17, 2023, Art. no. 2200792.

[24] J. H. Zhang et al., "Cascaded nanobeam spectrometer with high resolution and scalability," *Optica*, vol. 9, pp. 517–521, 2022.

[25] A. Poudel et al., "Spectrometer based on a compact disordered multi-mode interferometer," *Opt. Exp.*, vol. 31, pp. 12624–12633, 2023.

[26] W. Hartmann et al., "Waveguide-integrated broadband spectrometer based on tailored disorder," *Adv. Opt. Mater.*, vol. 8, 2020, Art. no. 1901602.

[27] W. Hadibrata et al., "Compact, high-resolution inverse-designed on-chip spectrometer based on tailored disorder modes," *Laser Photon. Rev.*, vol. 15, 2021, Art. no. 2000556.

[28] A. Mondal and K. Debnath, "Design of resolution-tunable neural network-based integrated reconstructive spectrometer," *IEEE Sensors J.*, vol. 22, no. 3, pp. 2630–2636, Feb. 2022.

[29] J. Xiong et al., "Dynamic brain spectrum acquired by a real-time ultraspectral imaging chip with reconfigurable metasurfaces," *Optica*, vol. 9, pp. 461–468, 2022.

[30] Z. Wang et al., "Single-shot on-chip spectral sensors based on photonic crystal slabs," *Nat. Commun.*, vol. 10, 2019, Art. no. 1020.

[31] C. Kim et al., "Mass production-enabled computational spectrometers based on multilayer thin films," *Sci. Rep.*, vol. 12, 2022, Art. no. 4053.

[32] Z. W. Cheng et al., "Generalized modular spectrometers combining a compact nanobeam microcavity and computational reconstruction," *Amer. Chem. Soc. Photon.*, vol. 9, pp. 74–81, 2022.

[33] H. H. Yoon et al., "Miniaturized spectrometers with a tunable van der Waals junction," *Science*, vol. 378, pp. 296–299, 2022.
[34] S. Nakashima, K. Sugioka, and K. Midorikawa, "Enhancement of resolution and quality of nano-hole structure on GaN substrates using the second-harmonic beam of near-infrared femtosecond laser," *Appl. Phys. A*, vol. 101, pp. 475–481, 2010.
[35] S. Bae et al., "Multifocal microlens arrays using multilayer photolithography," *Opt. Exp.*, vol. 28, pp. 9082–9088, 2020.
[36] D. Lee et al., "Pore-size reduction protocol for SiN membrane nanopore using the thermal reflow in nanoimprinting for nanobio-based sensing," *J. Biomed. Opt.*, vol. 19, 2014, Art. no. 051211.
[37] C. D. Vita et al., "Amorphous-silicon visible-light detector integrated on silicon nitride waveguides," *Opt. Lett.*, vol. 47, pp. 2598–2601, 2022.
[38] Y. Gao et al., "High-performance chemical vapor deposited graphene-on-silicon nitride waveguide photodetectors," *Opt. Lett.*, vol. 43, pp. 1399–1402, 2018.
[39] K. Wu, H. Zhang, Y. Chen, Q. Luo, and K. Xu, "All-silicon microdisplay using efficient hot-carrier electroluminescence in standard 0.18 μm CMOS technology," *IEEE Electron Device Lett.*, vol. 42, no. 4, pp. 541–544, Apr. 2021.
[40] K. K. Xu, "Silicon electro-optic micro-modulator fabricated in standard CMOS technology as components for all silicon monolithic integrated optoelectronic systems," *J. Micromechanics Microengineering*, vol. 31, 2021, Art. no. 54001.
[41] S. Qiu et al., "Ultrahigh-sensitivity label-free single mode-tapered multimode-single mode fiber U-shaped biosensor for Staphylococcus aureus detection," *Sensors Actuators B: Chem.*, vol. 375, 2023, Art. no. 1329227.